European Journal of Mechanics B/Fluids 36 (2012) 48–62

Contents lists available at SciVerse ScienceDirect

European Journal of Mechanics B/Fluids

journal homepage: www.elsevier.com/locate/ejmflu

Parametric study on a cylinder drag reduction using downstream undulating foil

Qing Xiao *, Wendi Liu, Jianxin Hu

Department of Naval Architecture and Marine Engineering, University of Strathclyde, Glasgow, G4 0LZ, UK

ARTICLE INFO

Article history:
Received 4 October 2011
Received in revised form
4 February 2012
Accepted 13 April 2012
Available online 25 April 2012

Keywords:
Cylinder drag reduction
Vortex interaction
Undulating foil

ABSTRACT

The motivation of this paper stems from our recent study [Q. Xiao, K. Sun, H. Liu, J.X. Hu, Computational study on near wake interaction between undulation body and a D-section cylinder, Ocean Eng. 38 (2011) 673–683] which shows that, for a flow system with a D-sectional cylinder combined with an undulating NACA0012 foil in the wake of a cylinder, cylinder drag force could be considerably reduced if the foil is properly placed in the cylinder wake. In this study, a further detailed parametric study on this coupled cylinder–undulating foil system is carried out by a numerical simulation. Particular interest is focused on how Reynolds number, the relative size of the foil to the cylinder, the foil undulating frequency, the wavelength and the gap between the cylinder and the foil affect the cylinder drag, lift force as well as foil thrust. For a range of flow and geometry parameters studied here, our results show that the maximum cylinder drag and the lift coefficient can be reduced as much as 57.4% and 63.3% as compared to the cylinder without the undulating foil. Foil thrust coefficient increases up to 4 times as compared to a single foil. Distinguishing itself from the conventional cylinder vortex control method, the coupled cylinder–undulating foil system provides new insights on the vortex control and suppression mechanism.

1. Introduction

The case of the vortex shedding control, either performed actively or passively while causing a reduction in the drag force of the cylinder, is a classic research topic due to their extensive applications in offshore engineering, such as marine pipeline and riser industry. Active or passive control is defined respectively based on whether if energy inputs are being supplied to the control system. One efficient passive control method proposed by previous researchers is to utilize the vortex splitter devices. (See review papers of Zdravkovich [1] and Choi et al. [2].) Within this category, commonly used devices include an attached or detached splitter plate [3–6], a small controlled stationary or rotating cylinder [7–11], a stationary foil [12] and an undulating foil [13]. Investigations showed that the flow structure of classic Karman vortex street in the cylinder wake is altered via the interfering of the added splitter plate. Such interaction also leads to either a diminished or an enhanced cylinder drag and peak lift force, depending on factors such as the size of splitter devices, the gap between the cylinder and the device and the particular Reynolds number.

Among mentioned papers, the study by Liao et al. [12] on the cylinder–foil system is of most relevance to our recent and present work. In their work, a numerical simulation is carried out to investigate the vortex interaction between a circular cylinder and a downstream stationary foil. The foil is placed with a non-zero transverse distance away from the cylinder center-line and a non-zero angle of attack. Various vortex structures are identified depending on the foil location in the downstream of the cylinder. The preferred vortex shedding frequency in the foil wake is found to be synchronized with the vortex shedding frequency of the upstream cylinder. Similar to Xiao et al. [13], the main focus of their study is on the propulsive phenomena of the downstream foil rather than the hydrodynamics effect on the upstream cylinder.

Vortex control is also successfully utilized by aquatic animal to enhance movement in water [14]. It is a well known fact that fish can efficiently propel themselves forward by taking the energy from their surrounded vortex field. [15–19], and examples abound when schools of fish are often spotted swimming in large water bodies, e.g. rivers, oceans. Other studies done on this aspect include papers by Gopalkrishnan et al. [20], Liao et al. [21,22] and Liao [23], Beal et al. [24], Eldredge and Pisani [25] and Xiao et al. [13].

Recent numerical work by Xiao et al. [13] on the interaction between an undulation NACA0012 foil and the wake of a D-section cylinder (see schematic diagram in Fig. 1) shows that the downstream undulation foil has a profound effect on the cylinder drag force and peak lift force depending on the gap ratio between the cylinder and the foil as well as the undulation frequency of the foil. Their results show that an optimal gap ratio of $L/c = 1.0$ is obtained at a non-dimensional undulation frequency $St_f = 0.16$ at which the cylinder drag coefficient reduces to 43% of that of a single cylinder. Here the non-dimensional undulating frequency is defined by the Strouhal number as $St_f = fA/U_\infty$ where A is the foil tail amplitude, f is the frequency and U_∞ is the incoming velocity. Apart from the impact of the undulating foil on the

* Corresponding author. Tel.: +44 141 5484779.
E-mail address: qing.xiao@strath.ac.uk (Q. Xiao).

0997-7546/$ – see front matter © 2012 Elsevier Masson SAS. All rights reserved.
doi:10.1016/j.euromechflu.2012.04.005

Nomenclature

CUF	Cylinder–undulation foil
CSF	Cylinder–stationary foil
SSC	Single semi-cylinder
U_∞	Free-stream velocity
D	Cylinder diameter
Re	Reynolds number
t	Instant time
T	Period of foil undulation
λ_f	Foil undulation wavelength
C_t	Thrust force coefficient
C_d	Drag force coefficient
C_l	Lift force coefficient
f_c	Cylinder vortex shedding frequency associated with CSF or CUF
f_n	Cylinder vortex shedding frequency associated with SSC
St_f	Foil Strouhal number
L	Distance between foil and cylinder
c	Foil chord length
f_f	Foil tail beat frequency
λ_c	Cylinder wake wavelength
A	Amplitude of foil tail.

cylinder drag force, the vortex interaction between the foil and the cylinder also plays a significant role in the propulsion performance of the downstream foil. Our earlier results also revealed that the thrust performance of the foil is improved with the presence of an upstream D cylinder.

Insights shed, however, are very limited due to the investigations conducted with a single fixed Reynolds number of $Re = 4.5 \times 10^4$ and the cylinder diameter being set equal to the foil chord length. The undulation foil wavelength is also numerically fixed at 1.15 of body length. These hypothetical values set under numerical conditions cannot be conclusively used to determine the general case, and in other words, results when applied to other cylinder–foil parameters are still ambiguous. In addition, most of the concentration is focused on the downstream foil propulsive behavior, rather than the upstream cylinder drag reduction. To rectify the problem, a systematic parametric study is carried out as the extension of above work in this subsequent study. Investigation encompasses a wide range of Reynolds number, different ratios of cylinder diameter over foil length and much wider gap ratios. Foil undulation wavelength is also changed as well as the undulating frequency to model the various fish kinematic undulation effect on the cylinder drag and lift force. As a result, the optimal parameters for the effective reduction on cylinder drag and peak lift would be systematically explored. We are expecting to gain new valuable insights on the cylinder vortex control mechanism by the undulating foil, which has never been investigated by known previous researchers.

2. Computational method

2.1. Description of problem

The problem configuration is depicted in Fig. 1. A semi-circular cylinder of diameter D is immersed in a uniform free-stream velocity of U_∞. An NACA0012 undulation foil with overall chord length c is placed at a distance L downstream of the cylinder and along the center-line. Four different systems are studied here, (1) Single Semi-circular Cylinder, represented as SSC, (2) single undulation foil, (3) coupled Cylinder–Stationary Foil denoted as CSF and (4) coupled Cylinder–Undulating Foil labeled as CUF.

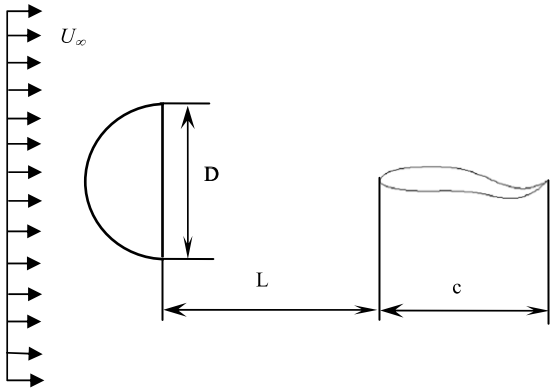

Fig. 1. Schematic diagram of flow configuration.
Source: From Xiao et al. [13].

The kinematic motion of undulation foil is determined by the foil centerline movement, which is based on the straightforward locomotion of a *Rana catesbeiana* larva, initially proposed by Wassersug and Hoff [26]. Such locomotion profile has been widely used by other researchers in fish swimming modeling [27–29]. The instantaneous lateral excursion of foil ($h(x, t)$) is defined as

$$h(x, t) = a(x) \sin\left[2\pi\left(\frac{x}{\lambda_f} - \frac{t}{T}\right)\right] \tag{1}$$

where $a(x)$ represents the lateral wave amplitude, x is the lengthwise coordinate measured from the fish head, t is the instantaneous time, λ_f is the wavelength and T is the undulation period.

The amplitude $a(x)$ is expressed as a sinusoidal equation as follows [29]:

$$a(x) = c \cdot \left[0.351 \cdot \sin\left(\frac{x}{c} - 1.796\right) + 0.359\right]. \tag{2}$$

For a coupled Cylinder–Undulating Foil system (CUF), the flow characteristics of cylinder or foil are determined by following three groups of parameters

(a) *Non-dimensional geometry parameters relevant to both foil and cylinder*. These include the gap ratio based on the foil chord length L/c, and the relative size of the foil and the cylinder D/c. Simulations are performed for a series of gap ratios (0.5, 1.0, 1.5, 2.0, 3.0 and 4.0) and D/c of 1.0, 2.0 and 3.0.

(b) *Kinematic parameters relevant to undulation foil* such as the non-dimensional frequency defined by Strouhal number as $St_f = fA/U_\infty$ and the foil non-dimensional wavelength λ_f. In all our computations, the amplitude $a(x)$ in Eq. (2) is specified and the maximum $a(x)$ at trailing edge is 0.022 m. The foil non-dimensional wavelength is increased from 0.8 to 1.2 and St_f varies from 0.16 to 0.48. Considering the interaction between the upstream cylinder and downstream foil, in order to control the cylinder vortex shedding effectively, the imposed foil undulating frequency St_f is expected to be comparable to the cylinder vortex shedding frequency without the downstream foil (St_c). Our preliminary simulation for the flow across a single D-sectional cylinder shows that, for the flow conditions explored in the present study, St_c varies from 0.25 to 0.3. Therefore, we can conclude with confidence that the St_f values studied here are appropriately selected.

(c) *The flow and geometry parameters characterizing the vortex shedding in the cylinder wake*. These parameters include Reynolds number based on the cylinder diameter, and free-stream velocity ($Re = \rho U_\infty D/\mu$) and the cylinder diameter

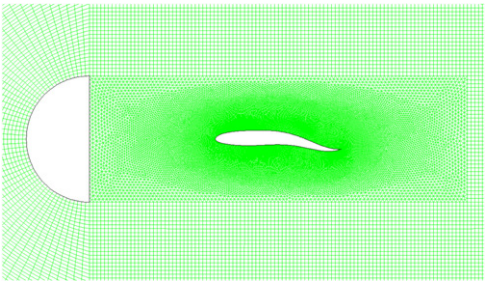

Fig. 2. Grid distribution near the cylinder and the foil.

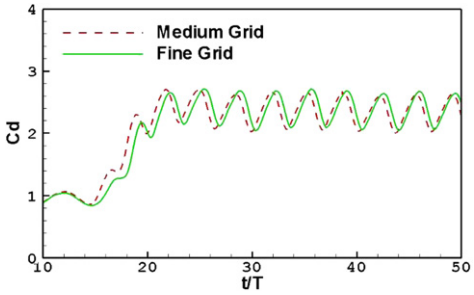

Fig. 3. Evolution of cylinder drag coefficient for combined cylinder–foil system (grid dependence test) $St_f = 0.32$; $Re = 45{,}000$ and $L/c = 2.0$.

D. As Zdravkovich [1] pointed out, the vortex shedding wavelength (λ_c) is solely determined by the cylinder diameter while the frequency is governed by both the Reynolds number and the diameter. In present computations, Reynolds number varies from 7500 to 45,000 systematically.

2.2. Numerical approach

The computations are carried out using a commercial CFD package—FLUENT. The details of the computational equations and the numerical method are presented by the authors in Ref. [13]. The governing equations describing the unsteady incompressible flow denoting the mass and momentum conservation are as follows:

$$\frac{\partial \rho}{\partial t} + \nabla \cdot (\rho \mathbf{u}) = 0$$

$$\frac{\partial (\rho \mathbf{u})}{\partial t} + \nabla \cdot (\rho \mathbf{u}\mathbf{u}) = -\nabla p + \nabla \cdot \tau \tag{3}$$

where ρ is the fluid density, $\mathbf{V}$ is the velocity vector, t is the instantaneous time, p is the pressure. For a Newtonian fluid, the viscous shear stresses is defined as

$$\tau_{\alpha\beta} = \mu(\partial_\alpha u_\beta + \partial_\beta u_\alpha) - \frac{2}{3}\mu\delta_{\alpha\beta}\partial_\alpha u_\alpha \tag{4}$$

with the dynamic viscosity μ.

Note that the finite volume method is used to discretize the above equations.

A second-order upwind scheme that is used for convective terms and diffusion-term discretization is applied with the second-order central-differencing scheme. Since dynamic mesh method in FLUENT is used to cope with the deforming mesh, implicit first order time-marching scheme is applied for the time marching. The solution procedure is based on a SIMPLE type segregated algorithm with coupled structure and unstructured mesh.

The grid quality affects the computed results accuracy since the pressure and viscous force on the cylinder and foil are integrated to obtain the cylinder drag, lift force and foil thrust. To accurately capture the near-wall vortices, very fine triangular grids are constructed in the wake of the cylinder and the near-wall area around the foil. A quadrilateral grid is generated within the rest part of computational domain to minimize the computational time as shown in Fig. 2. In the case of coupled system with undulating foil motion, the foil shape deforms at each time step. Dynamic mesh function in FLUENT is used, combined with the further developed problem-based User Defined Function to describe the motion of foil and re-compute the new mesh at each time step.

The computational domain extends 16 and 8 chord length in stream-wise (x) and translation (y) directions. Symmetric boundary conditions are imposed on the top and bottom computational domain. A uniform x-direction velocity is used as the inflow boundary condition, with $u = U_\infty$, $v = 0$ and $\partial p/\partial x = 0$. The outflow boundary condition is set as $\partial u/\partial x = 0$, $\partial v/\partial x = 0$ and $p = p_\infty$. On the moving foil surface, the velocity component in x direction (u) is equal to zero and v is specified by the kinematic equation (1).

2.3. Relevant parameters

To quantify the cylinder drag reduction, time-mean cylinder drag coefficient C_d and maximum instantaneous lift coefficient $C_l(t)$ are used. The drag coefficient C_d is defined as

$$C_d = \frac{\overline{F}_d}{\frac{1}{2}\rho U_\infty^2 D} \tag{5}$$

where $\overline{F}_d$ is the time-averaged force component of cylinder $X(t)$ in the stream-wise direction given by

$$\overline{F}_d = \frac{1}{T}\int_0^T X(t)dt \tag{6}$$

where T is the time period.

The instantaneous cylinder lift coefficient of $C_l(t)$ is determined by

$$C_l(t) = \frac{Y(t)}{\frac{1}{2}\rho U_\infty^2 D} \tag{7}$$

where $Y(t)$ is the instantaneous force component of cylinder in the vertical direction.

The undulation foil propulsion performance is quantified by the thrust coefficient C_t, which is defined as

$$C_t = \frac{\overline{F}_c}{\frac{1}{2}\rho U_\infty^2 c} \tag{8}$$

where $\overline{F}_c$ is the time-averaged value of the force component assuming the span-wise length of foil is 1.0.

To quantify the energy consumed by the undulating foil, foil efficiency is introduced and defined as below:

$$\eta = \frac{\overline{F}_{d^*} U_\infty}{\text{Power input}} \tag{9}$$

where the power input is obtained by integrating the pressure and viscous force on the foil surface.

$$\text{Power input} = \frac{1}{T}\int_0^T \oint f_p(x,t) \cdot \frac{\partial h(x,t)}{\partial t} dl\, dt \tag{10}$$

where $f_p(x,t)$ is the force acting on the foil surface and dl is the length of the surface element along the surface.

2.4. Validation and grid dependence test

The numerical methodology developed in this study, including the problem-based User Defined Function (UDF) to handle the unsteady moving boundary has been extensively validated for various unsteady bio-mimetic oscillating and undulation problems, such as the two-dimensional and three-dimensional flapping foil, the undulating NACA series foil and the undulating plate. (See detail in [13,30,31].)

Grid dependence test is carried out for a Coupled cylinder–Stationary Foil system (CSF) with two sets of mesh as medium grid (76,352 cells) and fine grid (83,818 cells). Instantaneous

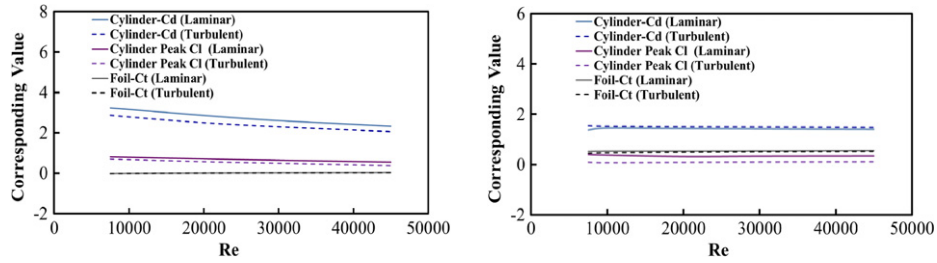

(a) Single cylinder and single undulation foil with $St_f = 0.32$.

(b) Cylinder–undulating foil system at $L/c = 1.0$; $St_f = 0.32$; $D/c = 1.0$; $\lambda_f = 1.15$.

Fig. 4. Comparison of turbulent and laminar flow results.

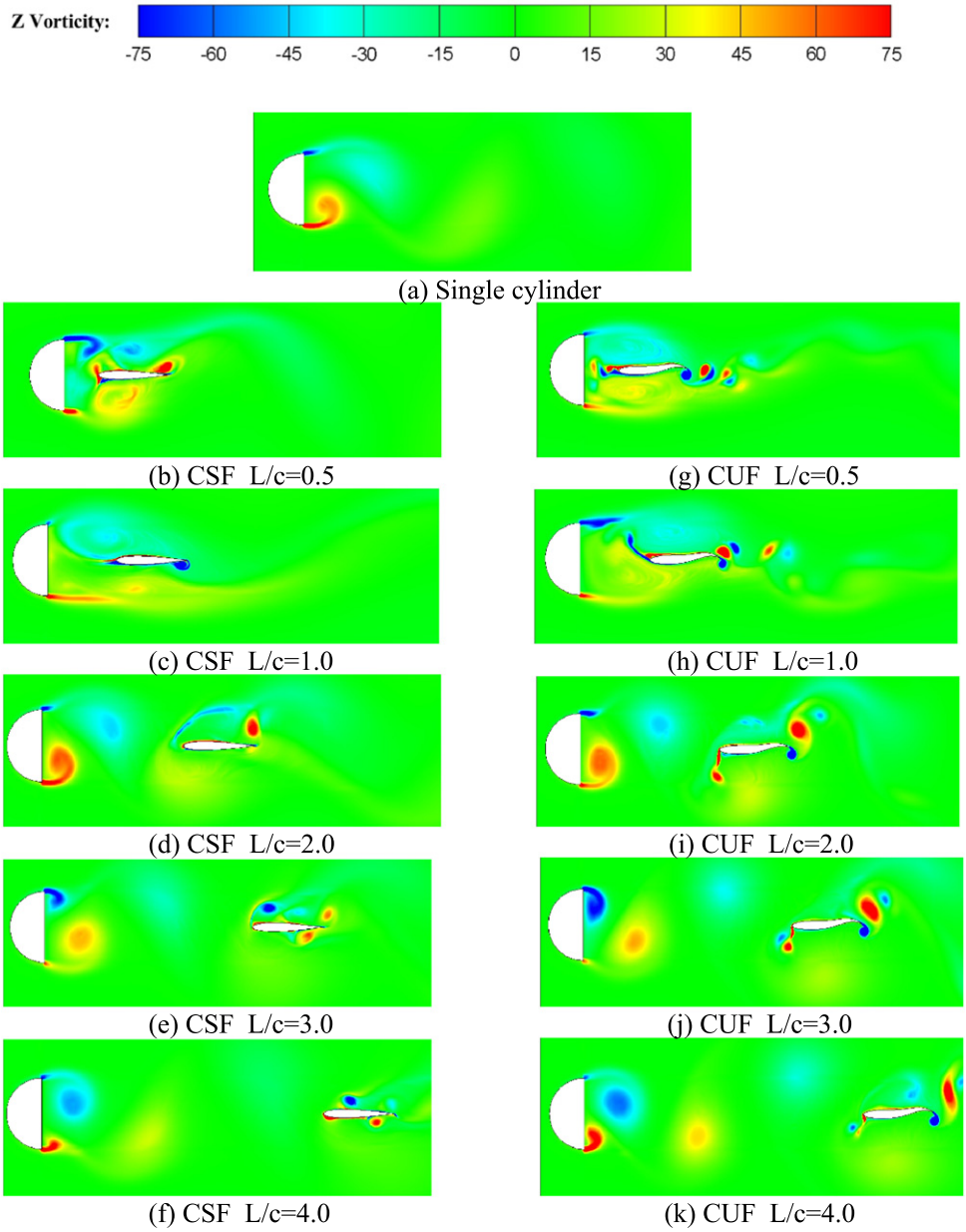

Fig. 5. Snapshot of vorticity contour for Cylinder–Stationary Foil system (CSF) and Cylinder–Undulation Foil system (CUF) at instantaneous time $t/T = 0.5$ ($St_f = 0.32$, $D/c = 1.0$ and $Re = 45{,}000$).

cylinder drag coefficients are compared in Fig. 3 for medium and fine grid. No significant difference is observed between the medium and fine mesh, for simplicity, all results presented hereafter are performed on the medium grid.

The maximum Reynolds number in the present study is 45,000, which is within the laminar turbulent transition regime. To judge whether a laminar solver can be used for the present study to cut computational cost, detailed comparison between the laminar

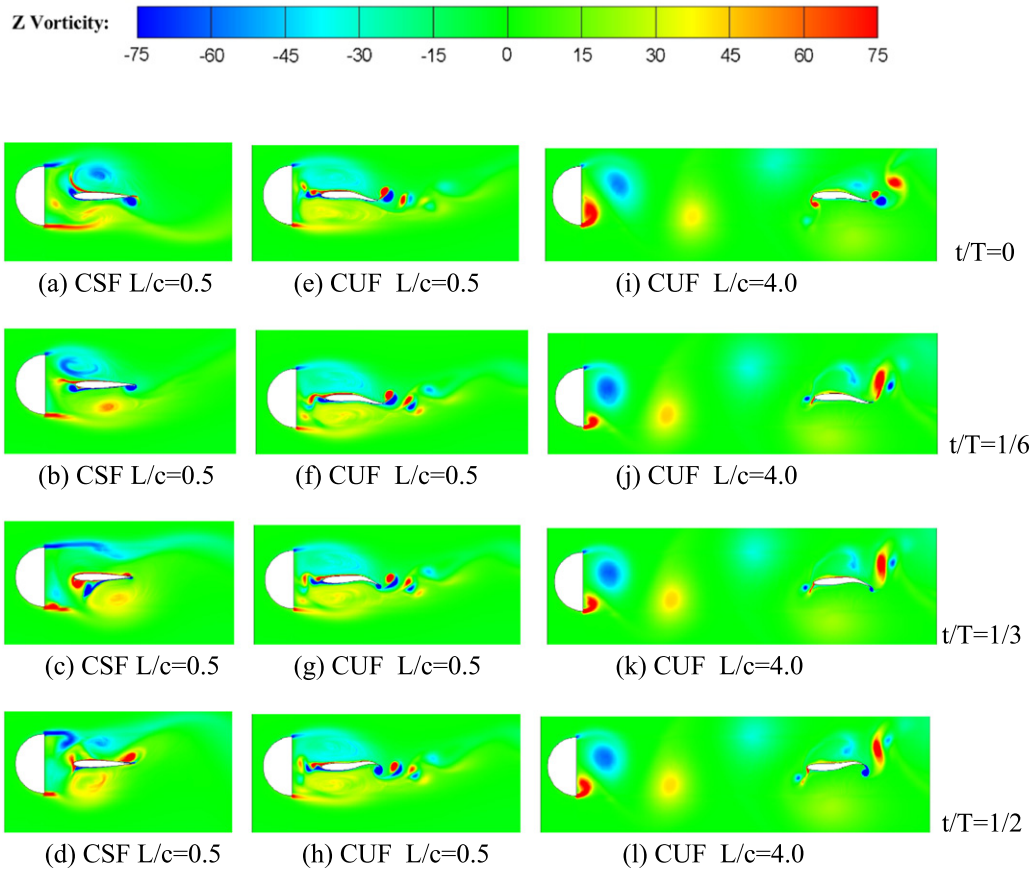

Fig. 6. Snapshot of vorticity contour within half foil undulating period for Cylinder–Stationary Foil and Cylinder–Undulation Foil systems ($St_f = 0.32$, $D/c = 1.0$ and $Re = 45{,}000$).

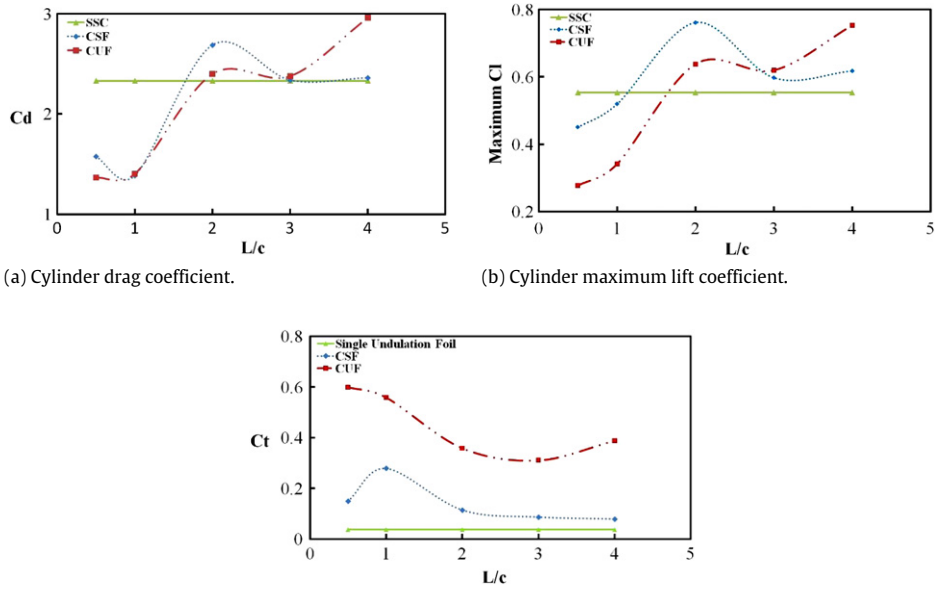

(a) Cylinder drag coefficient.

(b) Cylinder maximum lift coefficient.

(c) Foil thrust coefficient.

Fig. 7. Gap ratio effect on the time-mean cylinder drag coefficient (C_d), cylinder maximum lift coefficient (C_l) and foil thrust coefficient (C_t) with single cylinder, single foil and combined cylinder–foil system ($St_f = 0.32$, $Re = 45{,}000$) (a) Cylinder drag coefficient; (b) Cylinder maximum lift coefficient; (c) Foil thrust coefficient.

and turbulent results are performed for various problems, i.e. the flow across a single cylinder, the flow around a single undulating foil and the flow around a combined cylinder–foil system. The time-averaged cylinder drag force, peak cylinder lift force and foil thrust force are compared against each other in Fig. 4(a) and (b) for a range of Reynolds number ranging from $Re = 7500$ to 45,000. It is observed that, the deviation of turbulent results from its counterpart of laminar results is negligible. Considering the significant increase in computational time associated with the turbulent modeling, all simulations in the present study are

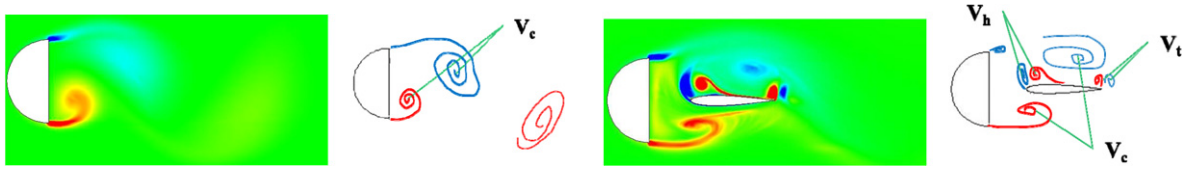

(a) Single cylinder. (b) Coupled cylinder–stationary foil ($L/c = 0.5$).

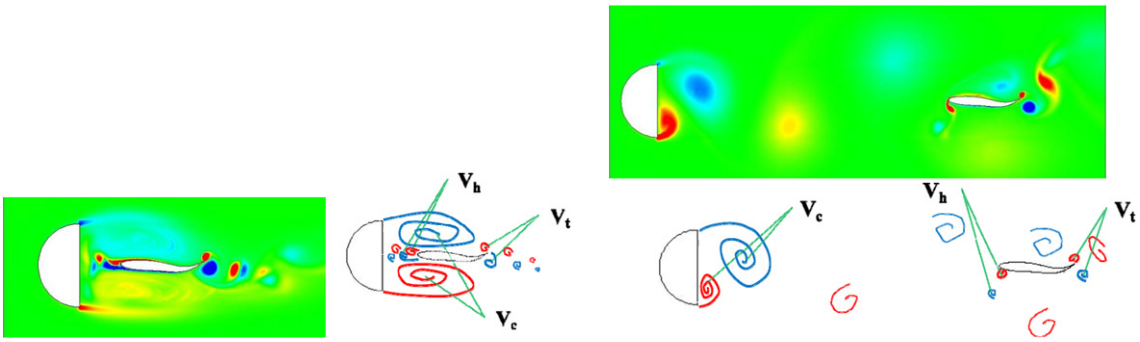

(c) Coupled cylinder–undulating foil ($L/c = 0.5$). (d) Coupled cylinder–undulating foil ($L/c = 4.0$).

Fig. 8. Vorticity contour and corresponding sketch for (a) Single cylinder; (b) Coupled cylinder–stationary foil ($L/c = 0.5$); (c) Coupled cylinder–undulating foil ($L/c = 0.5$); (d) Coupled cylinder–undulating foil ($L/c = 4.0$).

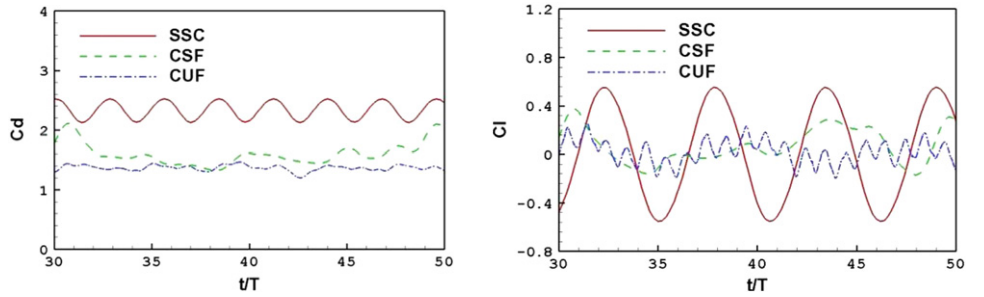

(a) Cylinder drag coefficient. (b) Cylinder lift coefficient.

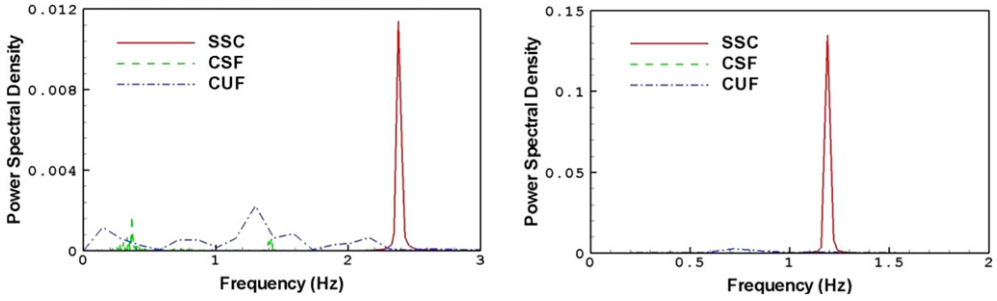

(c) Power spectral density (C_d). (d) Power spectral density (C_l).

Fig. 9. Instantaneous cylinder drag coefficient, lift coefficient and spectral analysis for SSC, CSF and CUF system. ($St_f = 0.32$, $L/c = 0.5$, $Re = 45{,}000$ and $D/c = 1.0$.)

performed based on a laminar solver to make best use of resources available.

3. Results and discussions

3.1. Mechanism of vortex control by the undulating foil

It is generally accepted that using an attached or detached splitter plate to control the cylinder vortical wake structure is achieved by reshaping the Von-Karman vortex street shedding in the near wake of cylinder. Particularly, by placing a splitter plate at a proper distance downstream of cylinder, the shear layer of upstream cylinder reattaches to the downstream plate, causing the formation of Karman vortex behind cylinder to be delayed. The vortex intensity in-between the cylinder and splitter plate significantly reduces and the wake pressure increases, leading to the reduced cylinder drag. This mechanism is well reinforced by the vorticity contours shown in Fig. 5(a)–(f) at the instantaneous time of $t/T = 0.5$ for various gap ratios ($L/c = \infty$ to 4.0) with a stationary foil–cylinder system (CSF). $L/c = \infty$ in the figure is used in reference to the single cylinder without foil.

As seen from Fig. 5(a)–(f), when a stationary foil is placed near cylinder such as $L/c = 0.5$ and 1.0, the development of Karman vortex in the cylinder wake is delayed further downstream. The evolution of vortices in an half foil undulating period (from $t/T = 0$ to 0.5) are displayed in Fig. 6(a)–(d) at $L/c = 0.5$

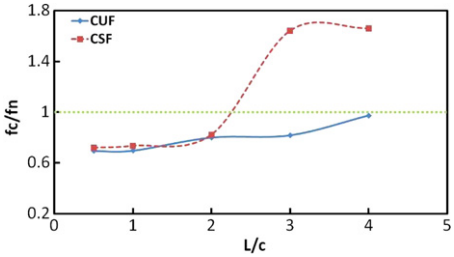

Fig. 10. Cylinder vortex shedding frequency ratio variation with gap ratio ($St_f = 0.32$, $Re = 45{,}000$ and $D/c = 1.0$).

and $D/c = 1.0$. It is clearly displayed in Fig. 6 that adding foil in the cylinder near wake moves the vortex core center further downstream, and weakens the vortices intensity. The time-mean cylinder drag coefficient and peak lift coefficients (C_d and C_l) presented in Fig. 7(a) and (b) clearly reflect such influences from the downstream foil. In fact, the drag coefficient and peak lift coefficient for CSF reduce about 32.23% and 18.66% relative to the single semi-cylinder (SSC) respectively.

However, the situation changes once the foil is placed further apart from the cylinder. From Fig. 7(a) and (b) on the time-averaged C_d and peak C_l, it is seen that, for $L/c \geq 2.0$, the cylinder drag and peak lift for CSF become larger than that of single cylinder, indicating that at these gap ratios, inserting the foil enhances the vortex shedding. Comparing Fig. 5(d) with Fig. 5(a), the vortex intensity between cylinder and foil at $L/c = 2.0$ obviously increased by exhibiting the shortened cylinder vortex shedding wavelength relative to SSC.

The above vortex control mechanism is also applied to cylinder–undulating foil system (CUF). However, apart from that, the vorticity contour with CUF in Fig. 5(g)–(k) and Fig. 6(e)–(l) at various instantaneous times and gap ratios show some specific features distinguishing from CSF system. Accompanying the foil undulation, there is a series of reversed Karman vortices generate in the vicinity of foil head with the upper row vortices rotating anti-clock-wise and the lower row vortices rotating clockwise (the V_h depicted in Fig. 8(b)). At small gap ratios ($L/c < 2.0$), such vortices periodically generate and move forward approaching to the upstream cylinder, interacts with Karman vortices shedding from the cylinder (V_c). Due to their rotating direction opposite to the Karman vortex, these vortices significantly reduce the Karman vortices strength and thus play an additional role on the weakening low pressure region in the cylinder wake. This further leads to an enhanced drag reduction effect as compared to the stationary foil. Such flow features are clearly represented by the vorticity contour plotted in Fig. 5(g)–(k). As seen in Fig. 7(a), the time-mean drag of CUF is slightly smaller than that of CSF, a profound decreasing peak lift coefficient with CUF is revealed in Fig. 7(b). For $L/c \geq 2.0$, similar observation is found for CUF and CSF, i.e. larger C_d and peak C_l are obtained than SSC system. The above findings on the cylinder drag reduction by vortices energy cancelation, via continuously releasing reversed Karman vortex, is of resemblance to the cylinder wake vortex structure control mechanism by imposing a rotating cylinder in the wake of upstream cylinder as found in [11].

When the gap ratio is further increased beyond 3.0, cylinder–foil systems obtain a higher C_d and C_l relative to SSC as displayed in Fig. 7(a) and (b), which is probably caused by another impact from the undulating foil. As discussed earlier, the releasing of reversed Karman vortex at the trailing edge of foil provides a positive contribution to the cylinder drag reduction. Apart from this, the interference between foil and cylinder is also via a continuous variation of actual vortex convecting downstream area induced by the undulating foil. Due to the vigorous variation of this area, the cylinder wake vorticity could be increased, and its effect on the cylinder drag reduction therefore becomes negative. It is obvious that, with a large gap between the foil and cylinder, the moving-forward reversed Karman vortex has little impact on the cylinder wake. However, the later mechanism associated with the increased cylinder drag dominates the flow, and thus an increased cylinder drag and peak lift is observed at large gaps.

The time-mean foil thrust coefficient (C_t) for single foil, coupled cylinder–stationary foil (CSF) and coupled cylinder–undulating foil (CUF) systems are compared in Fig. 7(c). Clearly, foil thrust increases for both CUF and CSF systems relative to single foil case, indicating that the downstream foil, either stationary or undulating, extracts energy directly from the cylinder's wake. The CUF thrust is also larger than that of CSF, leading to the conclusion that more energy is extracted through undulating foil.

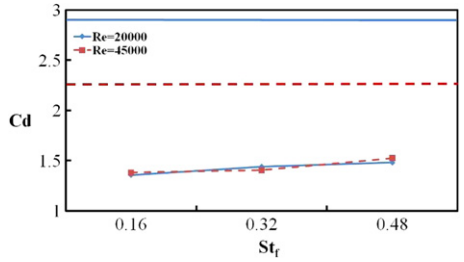

(a) Cylinder drag coefficient.

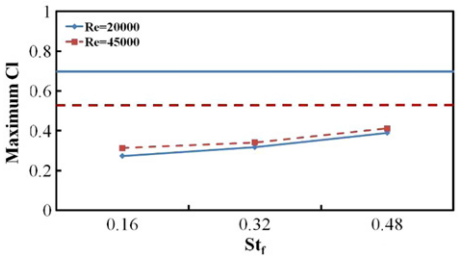

(b) Cylinder maximum lift coefficient.

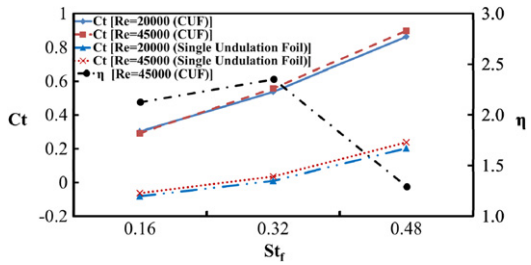

(c) Foil thrust coefficient and propulsion efficiency.

Fig. 11. Foil undulation frequency effect on time-mean cylinder drag coefficient (C_d), maximum cylinder lift coefficient (C_l) and foil thrust coefficient (C_t) ($D/c = 1.0$, $L/c = 1$, $\lambda_f = 1.15$) (a) Cylinder drag coefficient; (b) Maximum cylinder lift coefficient; (c) Foil thrust coefficient and propulsion efficiency. Horizontal solid line represents the corresponding value for SSC system at $Re = 20{,}000$ and horizontal dashed line represents the corresponding value for SSC system at $Re = 45{,}000$.

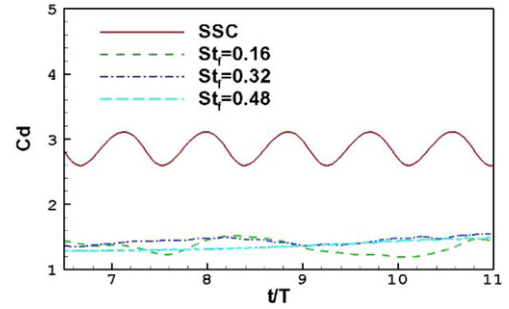

(a) Cylinder drag coefficient.

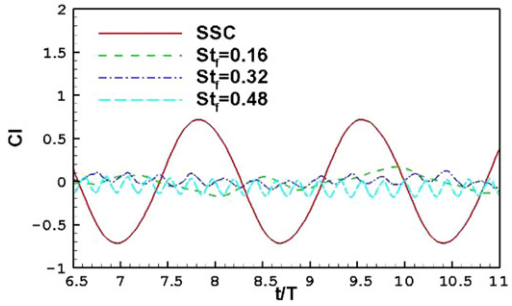

(b) Cylinder lift coefficient.

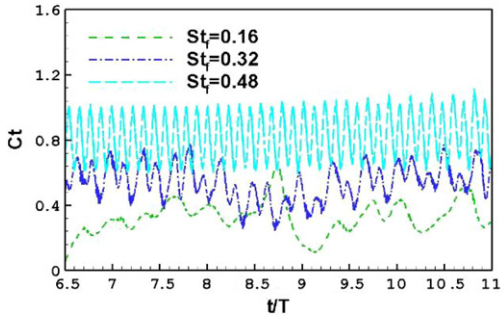

(c) Foil thrust coefficient.

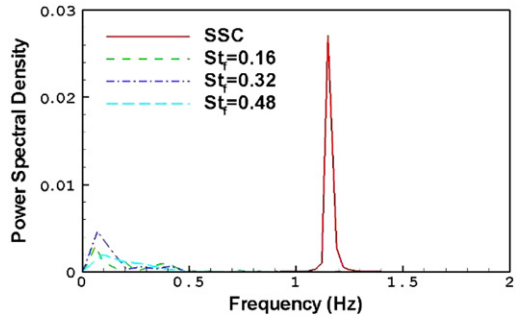

(d) Power spectral density (C_d).

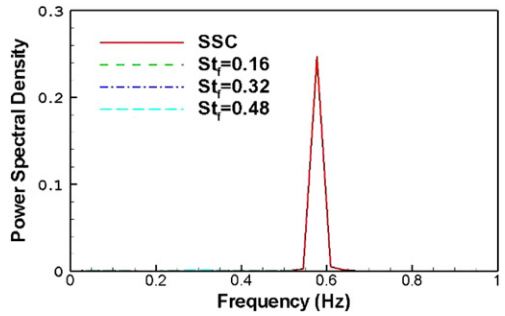

(e) Power spectral density (C_l).

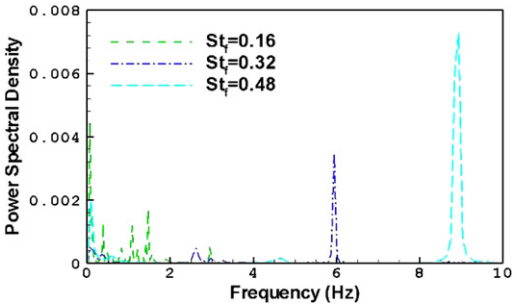

(f) Power spectral density (C_t).

Fig. 12. Instantaneous cylinder drag coefficient, cylinder lift coefficient, foil thrust coefficient and spectral analysis for various St_f ($D/c = 1.0$, $L/c = 1.0$, $\lambda_f = 1.15$ and $Re = 20{,}000$).

To quantify the foil effect on cylinder vortex shedding, the evolution of instantaneous cylinder drag and lift coefficients (C_d and C_l) are plotted in Fig. 9(a) and (b) at $L/c = 0.5$, $St_f = 0.32$ with $D/c = 1.0$ and $Re = 45{,}000$. As seen, the periodic variation of C_d and C_l associated with SSC are either eliminated or reduced by both CSF and CUF systems. These are also well reflected in Fig. 9(c) and (d) with the power spectral analysis using Fast Fourier Transformation (FFT) for the instantaneous C_d and C_l. A single dominant frequency, which corresponds to the vortex shedding with SSC, is replaced by the diffused frequency distribution with CSF and CUF as depicted in Fig. 9(c) and (d).

To better understand the gap ratio effect on the control of cylinder vortex shedding, Fig. 10 plots the vortex shedding frequency ratio against gap ratio, defined as f_c/f_n. Here f_c is the cylinder vortex shedding frequency associated with either CSF or CUF, and f_n is the natural frequency of cylinder vortex shedding without any downstream foil. It is clearly seen that at a value of $L/c < 2.0$ vortex shedding corresponding to CSF and CSU is suppressed with a smaller frequency relative to SSC indicated by $f_c/f_n < 1.0$ in Fig. 10. However, for $L/c > 2$, the shedding frequency is larger than SSC exhibiting the enhanced vortex shedding.

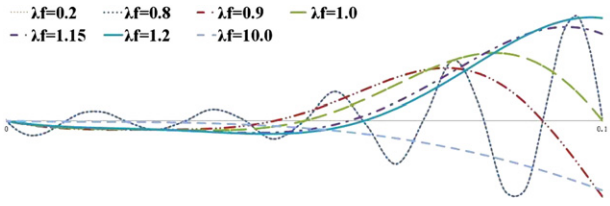

Fig. 13. Instantaneous foil central line trajectory at various foil wavelength λ_f ($t/T = 0.5$).

Obviously, the extent to which the cylinder wake is controlled by the undulating foil depends on the parameters of such coupled cylinder–foil system. As mentioned in Section 2.1, these parameters can be grouped into three categories. The effects of gap ratio are discussed above for a fixed Reynolds number of 45,000, with the undulating frequency $St_f = 0.32$ and foil undulating wavelength $\lambda_f = 1.15$. Also, the cylinder diameter is identical to the foil length ($D/c = 1.0$). In the following sections, computed results will be presented for a systematic parametric study for other cylinder and foil parameters.

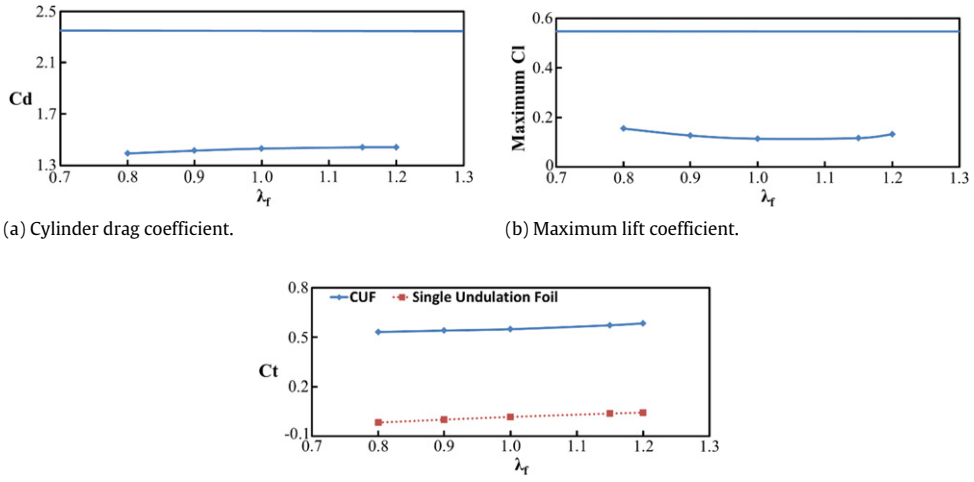

(a) Cylinder drag coefficient.

(b) Maximum lift coefficient.

(c) Foil thrust coefficient.

Fig. 14. Foil undulation wavelength effect on time-mean cylinder drag coefficient (C_d), maximum cylinder lift coefficient (C_l) and foil thrust coefficient (C_t) ($D/c = 1.0$, $L/c = 1$, $St_f = 0.32$ and $Re = 45{,}000$) (a) Cylinder drag coefficient; (b) Maximum cylinder lift coefficient; (c) Foil thrust coefficient. Horizontal solid line represents the corresponding value for SSC system.

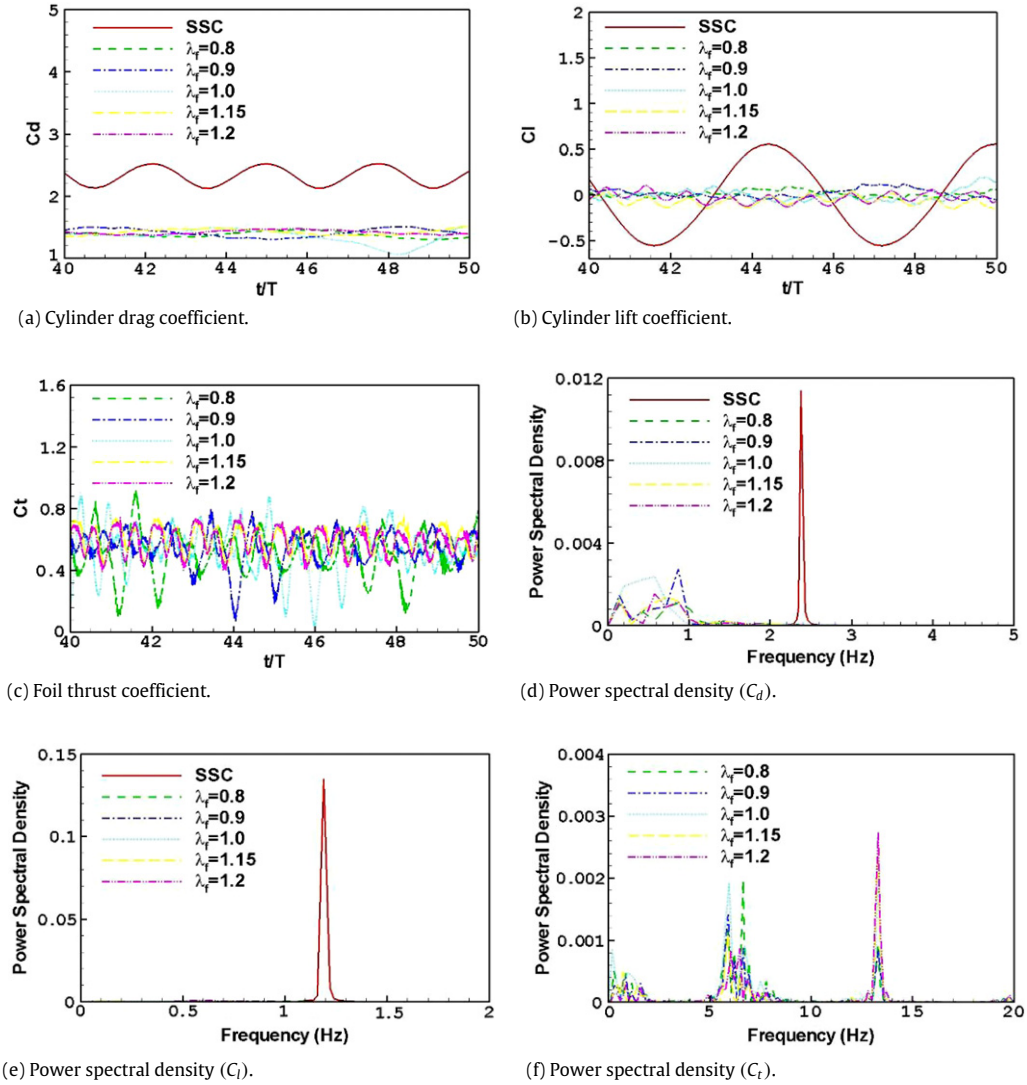

(a) Cylinder drag coefficient.

(b) Cylinder lift coefficient.

(c) Foil thrust coefficient.

(d) Power spectral density (C_d).

(e) Power spectral density (C_l).

(f) Power spectral density (C_t).

Fig. 15. Instantaneous cylinder drag coefficient, cylinder lift coefficient, foil thrust coefficient and spectral analysis for various λ_f ($St_f = 0.32$, $L/c = 1.0$ and $Re = 45{,}000$).

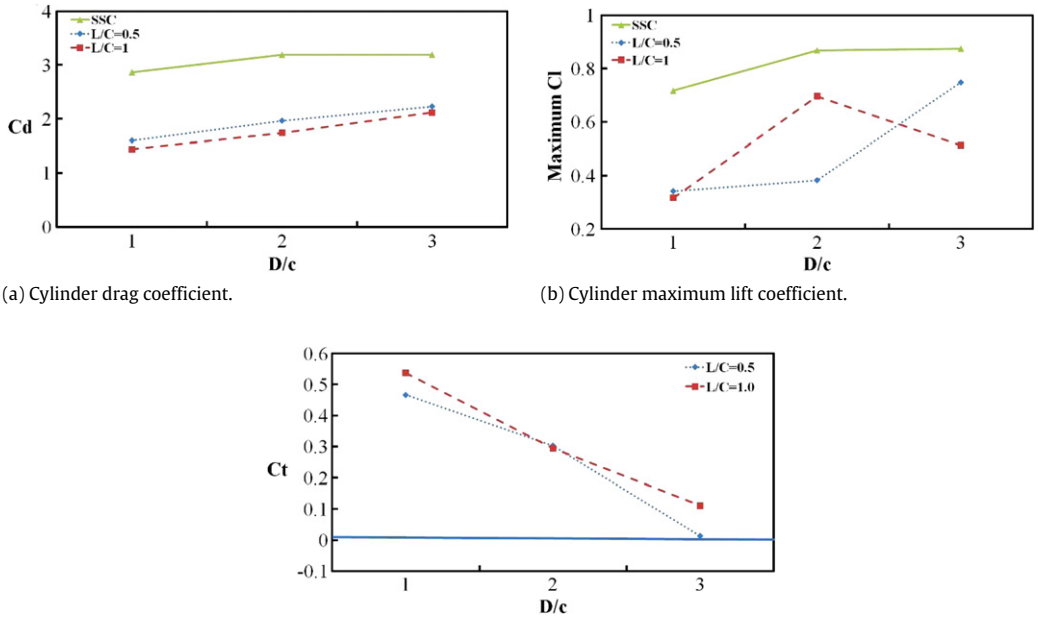

(a) Cylinder drag coefficient.

(b) Cylinder maximum lift coefficient.

(c) Foil thrust coefficient.

Fig. 16. Cylinder–foil size (D/c) effect on time-mean cylinder drag coefficient (C_d), maximum lift coefficient (C_l) and foil thrust coefficient (C_t) ($Re = 20{,}000$ and $St_f = 0.32$) (a) Cylinder drag coefficient; (b) Maximum lift coefficient; (c) Foil thrust coefficient.

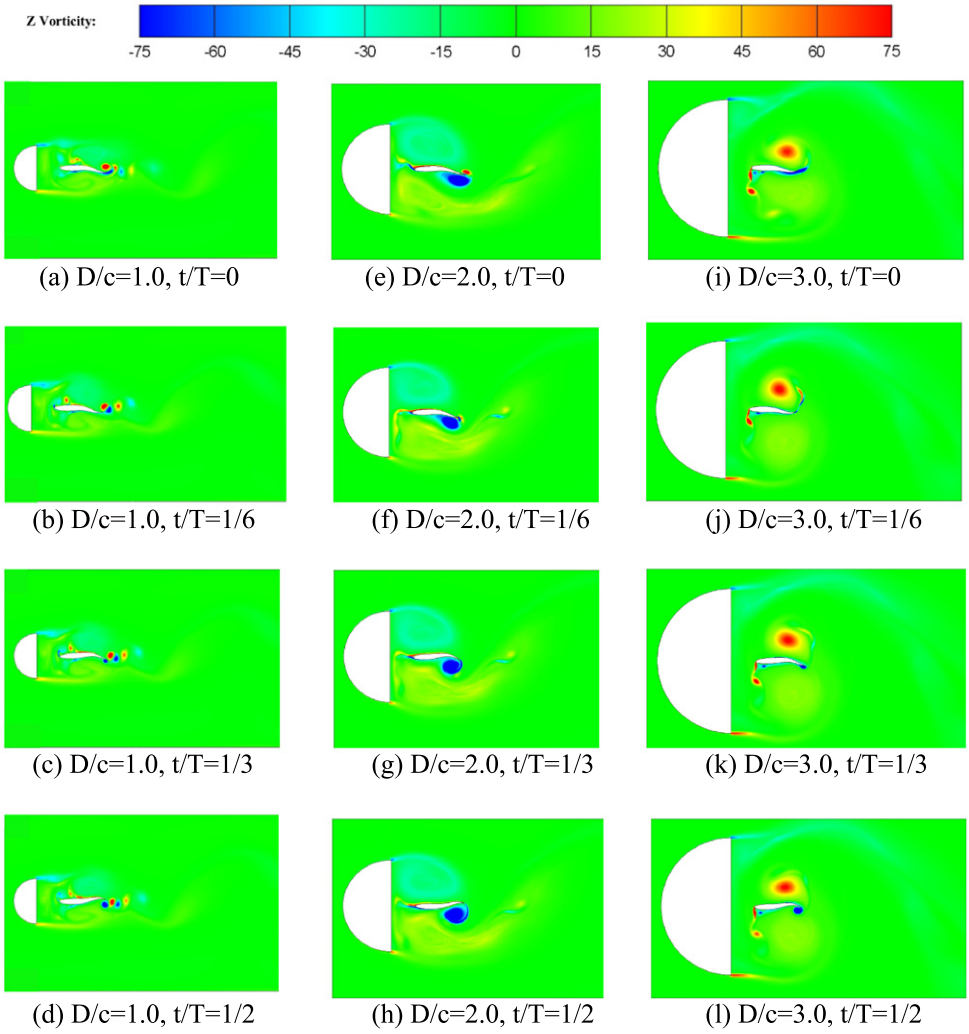

Fig. 17. Snapshot of vorticity contour in half foil undulating period for different D/c at $L/c = 0.5$, $St_f = 0.32$ and $Re = 20{,}000$.

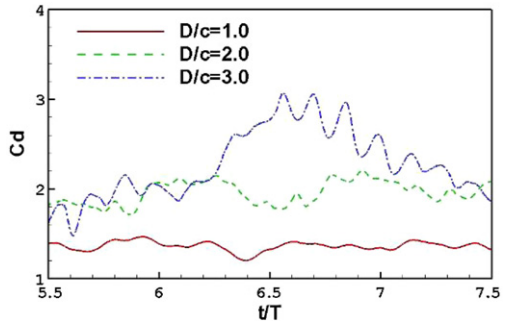

(a) Cylinder drag coefficient.

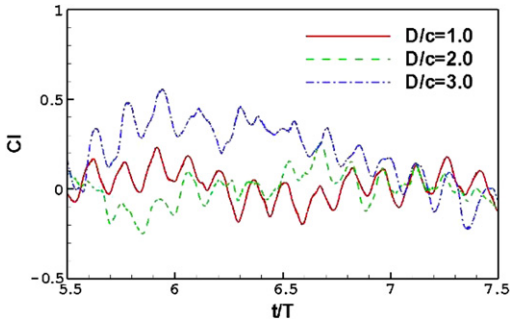

(b) Cylinder lift coefficient.

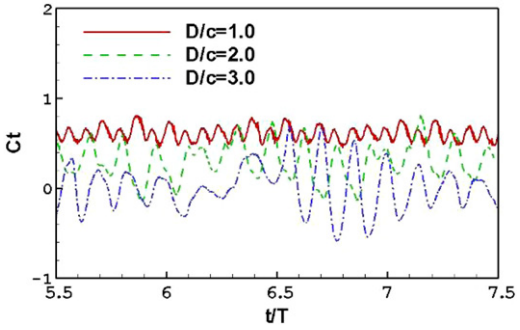

(c) Foil thrust coefficient.

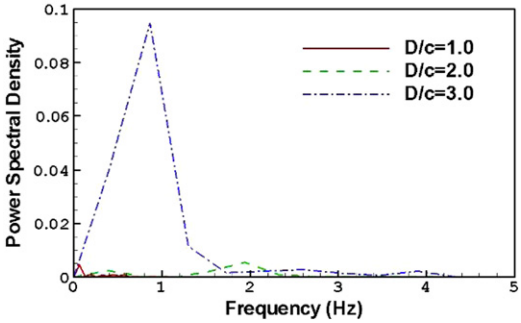

(d) Power spectral density (C_d).

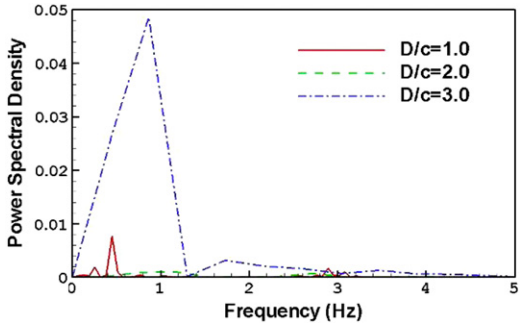

(e) Power spectral density (C_l).

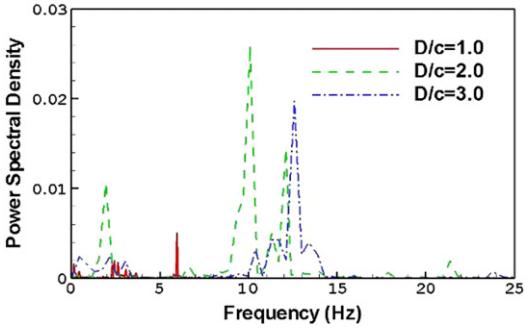

(f) Power spectral density (C_t).

Fig. 18. Instantaneous cylinder drag coefficient, cylinder lift coefficient and foil thrust coefficient and spectral analysis for various D/c ($St_f = 0.32$, $L/c = 0.5$ and $Re = 20{,}000$).

3.2. Foil parameter effect

3.2.1. Undulating frequency—Strouhal number (St_f)

The investigation of St_f effect on vortex control is carried out at two Reynolds numbers of 20,000 and 45,000 respectively. The gap ratio (L/c) and relative size ratio (D/c) are fixed at 1.0. Undulation foil wavelength λ_f is set at 1.15. Three Strouhal numbers are examined—$St_f = 0.16$, 0.32 and 0.48.

Fig. 11(a)–(c) show the time-mean cylinder drag coefficient, maximum lift coefficient and foil thrust coefficient for various St_f. As seen from the figures, the cylinder drag and lift for CUF system is significantly reduced as compared to SSC. Foil thrust coefficient, however, increases considerably relative to the single foil. This is caused by the efficient vortex energy extraction from the cylinder near the wake. Considering that the undulation locomotion of foil is prescribed, the input energy to maintain such motion and the overall system efficiency are two important parameters for the foil propulsive system. The definitions of input power and efficiency are defined in Eqs. (9) and (10) and the efficiency variation with various St_f is plotted in Fig. 11(c). As seen, at low undulating frequency such as $St_f = 0.16$ and 0.32, increasing undulating frequency leads to an enlarged propulsion efficiency. However, a further increasing St_f results in reduced efficiency, which is consistent with the extensively increased energy input while a relatively small thrust improvement at large St_f. For all cases tested, foil efficiency is larger than 1.0 indicating that the energy cost for undulating motion is effectively utilized by the foil to propel it forward. Since the focus of this paper is not on the undulating foil propulsion phenomena which are well addressed in detail in our recent paper Xiao et al. [13], further discussion on the foil propulsion efficiency will not be carried out in the following sections.

The instantaneous cylinder C_d, C_l and foil C_t and their spectral analysis results are displayed in Fig. 12 with $D/c = 1.0$, $L/c = 1.0$, $\lambda_f = 1.15$ and $Re = 20{,}000$. Clearly seen, the single dominant frequency related to the single cylinder vortex shedding frequency (SSC) disappears with the coupled cylinder–foil (SCF) system. Spectral analysis for foil thrust coefficient plotted in Fig. 12(f) shows the increased single dominant frequency with St_f. This is evidently related to the strengthened reversed Karman vortex structure in the downstream of undulating foil.

One striking feature noted is that, such cylinder drag reduction effect becomes weak with an increase of St_f. Apparently, the

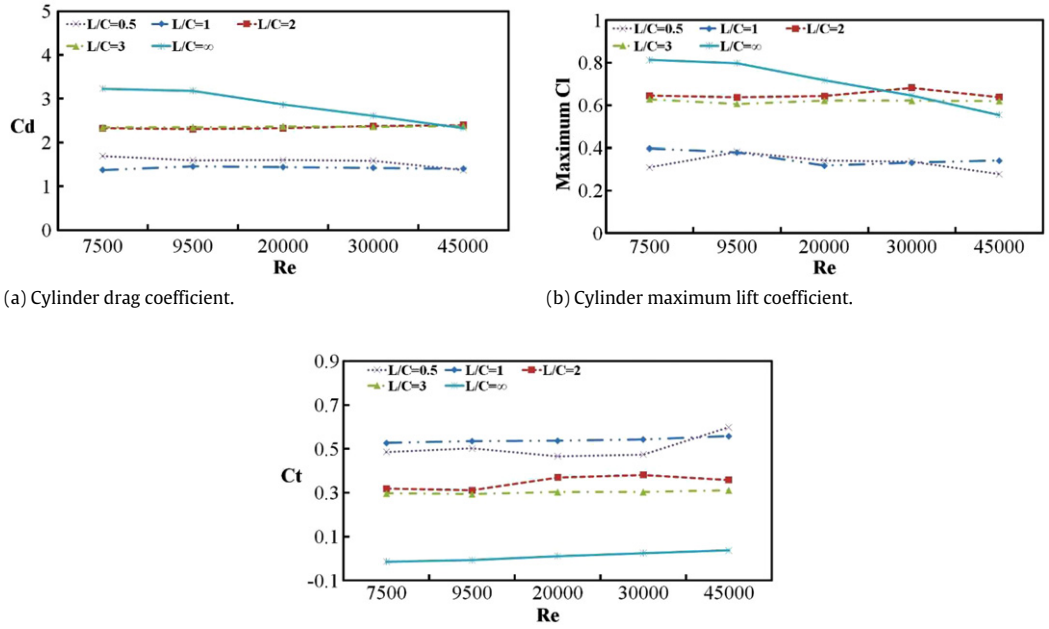

(a) Cylinder drag coefficient.

(b) Cylinder maximum lift coefficient.

(c) Foil thrust coefficient.

Fig. 19. Reynolds number effect on the time average cylinder drag coefficient, maximum lift coefficient and foil thrust coefficient ($St_f = 0.32$ and $D/c = 1.0$) (a) Cylinder drag coefficient; (b) Maximum lift coefficient; (c) Foil thrust coefficient.

interference between the foil and cylinder increases with St_f. As it is pointed out earlier in Section 3.1, there are two main mechanisms which the downstream foil interacts with the upstream cylinder. The first mechanism is the released reversed Karman vortex street at the head of foil which suppresses the cylinder wake vortex intensity. The other mechanism is the modifying of actual vortex convection area in the downstream direction. With added foil, the vortex convection area reduces, and delays the vortex convection speed, and extends the wake low pressure region, and thus increases cylinder drag. Higher St_f means the quick variation of foil shape and more frequent variation of flow convecting area. Increasing St_f apparently enhances the above two effects simultaneously, leading to the drag and maximum lift force of CUF approaching to SSC as shown in Fig. 11(a) and (b).

3.2.2. Undulating wavelength (λ_f)

Apart from the undulating frequency St_f, foil wavelength λ_f is another important parameter characterizing the locomotion of foil. Foil exhibits more flexibility with small λ_f as seen from the foil center-line trajectory plot in Fig. 13. The time-mean drag coefficient, maximum lift coefficient and the foil thrust coefficient variation with λ_f are presented in Fig. 14(a)–(c) at $Re = 45{,}000$ with $St_f = 0.32$, $L/c = 1.0$ and $D/c = 1.0$.

The cylinder drag and maximum C_l reduction are observed for all wavelengths. However, observation varies slightly with minor changes in λ_f. The best achievement for peak C_l reduction is at $\lambda_f = 1.0$ while it is changed to 1.2 for drag reduction. Increasing wavelength has the similar impact as St_f on the foil thrust enhancement, i.e. C_t increases monotonically with λ_f. Another similar parameter commonly used by other researchers on the foil propulsion problem is the undulating wave number, which is defined as $1/\lambda_f$. Previous studies on the wave number impact on the propulsion performance show that the thrust force decreases with wave number [32], which is consistent with our present results.

The evolution of instantaneous cylinder drag, maximum lift coefficient and foil thrust coefficient and their spectral analysis are shown in Fig. 15. For all wavelength studied here, the periodic feature of cylinder drag and lift coefficient becomes un-discernable, especially for the drag coefficient curve, reflecting the elimination of Karman vortex street in the cylinder wake.

3.3. Cylinder parameters

It is well known that the two key flow parameters characterizing single cylinder vortex shedding wake are vortex shedding frequency f_c and wavelength λ_c. The vortex shedding wavelength λ_c only depends on the cylinder diameter while the frequency f_c varies with incoming flow velocity (cylinder Reynolds number Re) and the cylinder diameter [23] The causes of the impact of undulating foil on the cylinder wake vortex interaction are therefore focused on these two aspects.

3.3.1. Relative cylinder–foil size (D/c)

Three sets D/c ($D/c = 1, 2$ and 3) are considered, corresponding to uncoupled cylinder vortex shedding wavelength λ_c of 0.2 m, 0.41 m and 0.64 m respectively. Gap ratio between cylinder and foil is fixed as $L/c = 0.5$ and 1. Reynolds number is 20,000, foil undulation frequency St_f is 0.32 and wavelength $\lambda_f = 1.15$.

Fig. 16 shows the time-mean cylinder drag coefficient, maximum lift coefficient and foil thrust coefficient varying with D/c for SSC and CUF systems at gap ratio of $L/c = 0.5$ and 1. The corresponding instantaneous cylinder drag coefficient, lift coefficient and foil thrust coefficient and their spectral analysis are shown in Fig. 18. Cylinder drag for CUF system significantly reduces as seen from Fig. 16(a). However, it approaches to the corresponding single cylinder value with increase of cylinder diameter or more specifically the cylinder vortex shedding wavelength λ_c. The maximum lift coefficient plotted in Fig. 16(b) shows the similar trend at $L/c = 1.0$. At $L/c = 0.5$, however, lift coefficient climbs up first from $D/c = 1.0$ to $D/c = 2.0$ and then decreases at $D/c = 3.0$. Foil thrust coefficient shown in Fig. 16(c) presents a declining trend of C_t with D/c. For three D/c studied here, though the coupled system C_t is larger than that of single foil, it is anticipated that the CUF foil thrust will drop below single foil value if D/c is increased further.

The snapshot of vorticity contours in half foil undulating period displayed in Fig. 17 clearly reflect above findings. When the

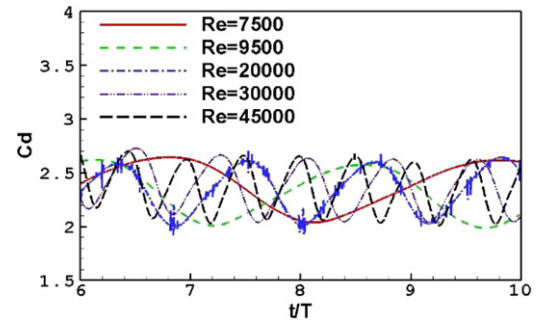

(a) Cylinder drag coefficient.

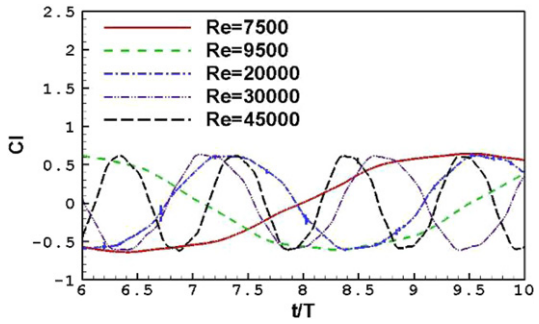

(b) Cylinder lift coefficient.

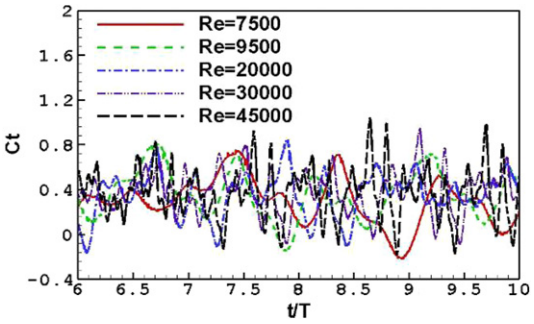

(c) Foil thrust coefficient.

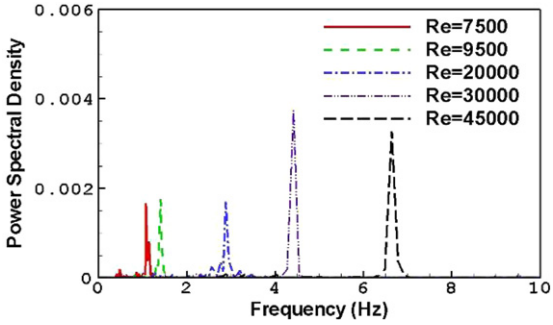

(d) Power spectral density (C_d).

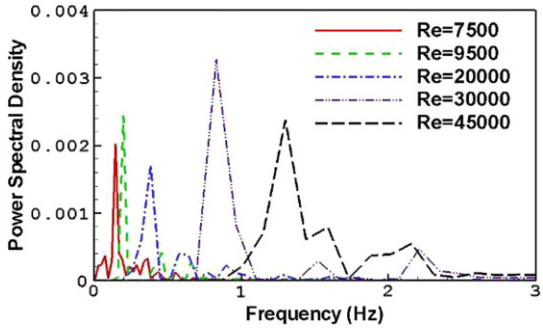

(e) Power spectral density (C_l).

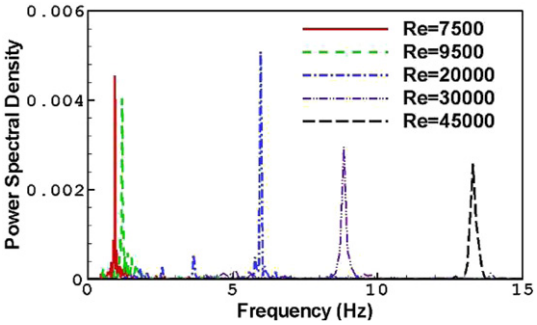

(f) Power spectral density (C_t).

Fig. 20. Instantaneous cylinder drag coefficient, cylinder lift coefficient, foil thrust coefficient and spectral analysis for various Reynolds number ($St_f = 0.32$ and $L/c = 0.5$).

cylinder size is comparable to undulating foil length (i.e. $D/c = 1.0$), the vortex shedding in the cylinder wake is effectively delayed by the downstream foil, leading to the cylinder drag reduction. At the same time, a series of reversed Karman vortex street form in the downstream wake of foil tail, which causes an enhanced foil's thrust force as compared to single foil. However, increasing D/c to 2.0, the SSC cylinder vortex shedding wavelength (λ_c) increases and the low pressure regime in the cylinder wake is enlarged and extended further downstream. The moving-forward reversed Karman vortex lessens its impact on the energy extraction from cylinder shedding Karman vortex street, as these vortices locates too far apart from the cylinder shedding Karman vortex. Meanwhile, the reversed Karman vortex releasing from the foil tail becomes diluted. The Above phenomenon becomes more and more significant when D/c increases from 2.0 to $D/c = 3.0$. The shortened cylinder vortex core distance indicates a vortex shedding enhancement. Clearly seen from Fig. 17(i)–(l) at $D/c = 3.0$, no reversed Karman vortex street appears in the foil wake. The computed results clearly indicate that, the best performance for the suppression cylinder vortex shedding is achieved when the foil length is comparable to the cylinder diameter.

3.3.2. *Reynolds number* (*Re*)

To investigate the Reynolds number effect, four different groups are studied at various gap ratios of $L/c = 0.5$, 1, 2 and 3. In each group, five different Reynolds numbers ($Re = 7500$, 9500, 20,000, 30,000 and 45,000) are examined at fixed $St_f = 0.32$.and $\lambda_f = 1.15$. The cylinder diameter is identical to the foil length.

The variation of CUF cylinder drag coefficient against the Reynolds number is small as compared to SSC ($L/c = \infty$) as seen from Fig. 19(a). However, drag coefficient C_d for SSC system decreases with an increase in Reynolds number. This results in CUF drag reduction effect to become weaker, and on top of that causing changes to drag to increase at $Re = 45{,}000$ with large gap ratios of $L/c = 2$ and 3. Similar observation is found on the maximum lift coefficient variation with Reynolds number shown in Fig. 19(b). Based on definition of *Re*, increasing Reynolds number can be achieved by increasing incoming velocity U_∞ if the cylinder diameter is fixed. To remain a constant foil Strouhal number St_f, the foil undulating frequency f_f must be increased when Reynolds number increases. As discussed in Section 3.1, increasing f_f causes more severe variation of cylinder vortex shedding convecting area, which may cause the drag to increase if f_f becomes too large. At large gap ratios, a larger CUF drag coefficient and peak lift

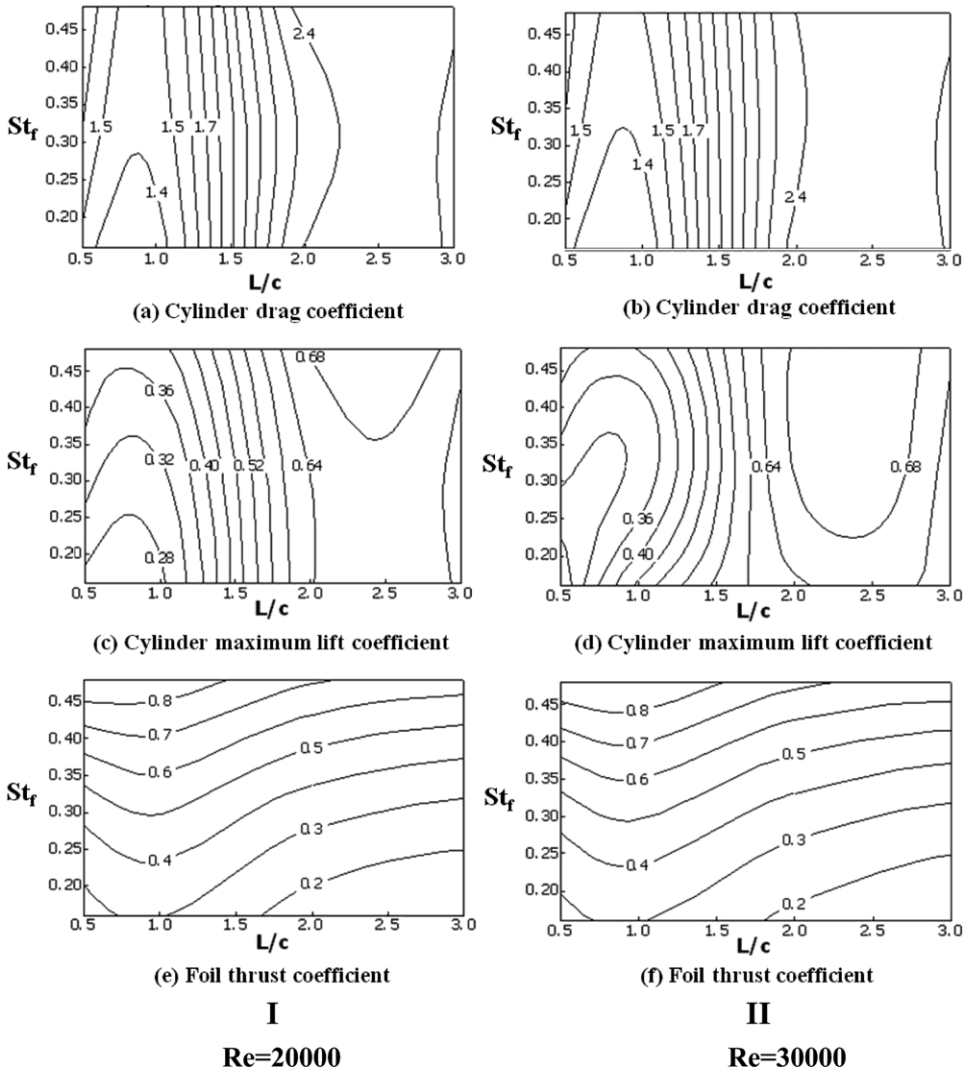

Fig. 21. Iso-line contour for time-mean cylinder drag coefficient, cylinder maximum lift coefficient and foil thrust coefficient at $Re = 20{,}000$ and $Re = 30{,}000$.

coefficient than that of SSC are good indications on the above conjecture. Note that the foil thrust coefficient, C_t, does not change with Reynolds number. Thrust coefficients of CUF are larger than that of single foil for all Reynolds numbers and gap ratios (see Fig. 19).

The evolution of instantaneous cylinder drag coefficient, maximum lift coefficient and foil thrust coefficient are shown in Fig. 20(a)–(c) along with their corresponding spectral analysis in Fig. 20(d)–(f). It is clearly seen that the effect of Reynolds number on the maximum C_d and C_l are insensible. However, increasing Re enlarges the instantaneous coefficients' frequency which is presented in both plots for instantaneous coefficients distribution and their power spectral analysis. This is due to the fact that rising in-coming flow velocity causes the quick cylinder vortex shedding. The wavelength remains the same irrespective of a Re variation.

3.4. Optimized parameters for VIV suppression

A series of parametric studies on the cylinder vortex control are presented above. They are summarized with iso-contour lines in Fig. 21 for $Re = 20{,}000$ and 30,000.

The lowest drag coefficient is observed at gap ratio L/c of 1.0 and undulating foil frequency St_f of 0.16–0.3. The smallest cylinder peak lift coefficient is influenced by the Reynolds number. At $Re = 20{,}000$, the lift coefficient reaches the minimum value at around $L/c = 1.0$ and St_f of 0.16–0.20, while the gap ratio for the minimum Cl moves to lower L/c equal to 0.5 at $Re = 30{,}000$. The maximum foil thrust coefficient is observed with larger foil undulating frequency St_f of 0.45 at $L/c = 1.0$. For the purpose of cylinder vortex suppression, the optimal parameters are the gap ratio L/c equal to 1.0 and the foil undulates with frequency St_f of 0.16. With these parameters, the reduction on maximum cylinder drag and lift coefficient is expected to reach as much as about 57.4% and 63.3% respectively relative to a single cylinder. Foil thrust coefficient is enhanced to 4 times as compared to a single foil.

4. Conclusions

This numerical study examines the potential of cylinder wake vortex control using a downstream undulating foil. It distinguishes itself considerably from our recent paper [13], which focuses on the propulsion performance enhancement of undulating foil by extracting energy from the upstream cylinder wake. The present investigation covers a much wider range of kinematic and geometric parameters of this coupled cylinder–foil system, such as the foil undulating frequency St_f, wavelength (λ_f) and the gap ratio (L/c) and cylinder–foil relative size (D/c). It aims for obtaining an optimal parametric range to achieve a significant cylinder drag

reduction, which is impossible to be accomplished by our earlier study on the limited parameters. Our results show that the proper placement of foil, with its chord length equal to the upstream cylinder diameter, can result in a suppression of cylinder vortex shedding and an improvement in downstream foil propulsion. The detailed flow field analysis reveals that, such benefit is strongly linked to the interaction between the cylinder wake vortex and the reversed Karman vortex street, which is shedding continuously at the foil leading edge associated with foil undulation locomotion. This new finding undetected by preceding investigations prompts further study in the near future.

References

[1] M.M. Zdravkovich, Review and classification of various aerodynamic and hydrodynamic means for suppressing vortex shedding, J. Wind Eng. Ind. Aerodyn. 7 (1981) 145–189.
[2] H. Choi, W.P. Jeon, J. Kim, Control of flow over a bluff body, Annu. Rev. Fluid Mech. 40 (2008) 113–139.
[3] K. Kwon, H. Choi, Control of laminar vortex shedding behind a circular cylinder using splitter plates, Phys. Fluids 8 (1996) 479–486.
[4] J.Y. Hwang, K.S. Yang, S.H. Sun, Reduction of flow-induced forces on circular cylinder using a detached splitter plate, Phys. Fluids 15 (2003) 2433–2436.
[5] C.J. Apelt, G.S. West, The effects of wake splitter plates on bluff-body flow in the range $10^4 < Re < 5 \times 10^4$. Part 2, J. Fluid Mech. 71 (1975) 145–160.
[6] J. Apelt, G.S. West, A. Szewczyk, The effects of wake splitter plates on bluff-body flow in the range $10^4 < Re < 5 \times 10^4$. Part 1, J. Fluid Mech. 61 (1973) 187–198.
[7] P.J. Strykowski, K.R. Sreenivasan, On the formation and suppression of vortex 'shedding' at low Reynolds numbers, J. Fluid Mech. 218 (1990) 71–107.
[8] M. Farhadi, K. Sedighi, E. Fattah, Effect of a splitter plate on flow over a semi-circular cylinder, J. Aerosp. Eng. 224 (Part G) (2009) 321–330.
[9] M.D. Symans, M.C. Constantinou, Semi-active control systems for seismic protection of structures: state-of-the-art review, Eng. Struct. 21 (1999) 469–487.
[10] S. Mittal, B. Kumar, Flow past a rotating cylinder, J. Fluid Mech. 476 (2003) 303–334.
[11] J. Li, J. Sun, B. Roux, Numerical study of an oscillating cylinder in uniform flow and in the wake of an upstream cylinder, J. Fluid Mech. 237 (1992) 457–478.
[12] Q. Liao, G.J. Dong, X.Y. Lu, Vortex formation and force characteristics of a foil in the wake of a circular cylinder, J. Fluids Struct. 19 (2004) 491–510.
[13] Q. Xiao, K. Sun, H. Liu, J.X. Hu, Computational study on near wake interaction between undulation body and D-section cylinder, Ocean Eng. 38 (2011) 673–683.
[14] K. Streitline, G.S. Triantafyllou, M.S. Triantafyllou, Efficient foil propulsion through vortex control, AIAA J. 34 (1996) 2315–2319.
[15] C.M. Breder, Vortices and fish schools, Zoologica 50 (1965) 97–114.
[16] D. Weihs, Hydromechanics of fish schooling, Nature 241 (1973) 290–291.
[17] P.W. Webb, Entrainment by river chub Nocomis micropogon and smallmouth bass micropterus dolomieu on cylinders, J. Exp. Biol. 201 (1998) 2403–2412.
[18] J. Herskin, J.F. Steffensen, Energy savings in sea bass swimming in a school: measurements of tail beat frequency and oxygen consumption at different swimming speeds, J. Fish Biol. 53 (1998) 366–376.
[19] S.G. Hinch, P.S. Rand, Optimal swimming speeds and forward-assisted propulsion: energy-conserving behaviors of upriver-migrating adult salmon, Can. J. Fish. Aquat. Sci. 57 (2000) 2470–2478.
[20] R. Gopalkrishnan, M.S. Triantafyllou, G.S. Triantafyllou, D. Barrett, Active vorticity control in a shear flow using a flapping foil, J. Fluid Mech. 274 (1994) 1–21.
[21] J.C. Liao, D.N. Beal, G.V. Lauder, M.S. Triantafyllou, Fish exploiting vortices decrease muscle activity, Science 302 (2003) 1566–1569.
[22] J.C. Liao, D.N. Beal, G.V. Lauder, M.S. Triantafyllou, The Karman gait: novel kinematics of rainbow trout swimming in a vortex street, J. Exp. Biol. 206 (2003) 1059–1073.
[23] J.C. Liao, A review of fish swimming mechanics and behaviour in altered flows, Phil. Trans. R. Soc. Ser. B 362 (2007) 1973–1993.
[24] D.N. Beal, F.S. Hover, M.S. Triantafyllou, J.C. Liao, G.V. Lauder, Passive propulsion in vortex wakes, J. Fluid Mech. 549 (2006) 385–402.
[25] J.D. Eldredge, D. Pisani, Passive locomotion of a simple articulated fish-like system in the wake of an obstacle, J. Fluid Mech. 607 (2008) 279–288.
[26] R. Wassersug, K. Hoff, The kinematics of swimming in anuran larvae, J. Exp. Biol. 119 (1985).
[27] H. Liu, R.J. Wassersug, K. Kawachi, A computational fluid dynamics study of tadpole swimming, J. Exp. Biol. 199 (1996) 1245–1260.
[28] H. Liu, R.J. Wassersug, K. Kawachi, The three-dimensional hydrodynamics of tadpole locomotion, J. Exp. Biol. 200 (1997) 2807–2819.
[29] H. Liu, K. Kawachi, A numerical study of undulatory swimming, J. Chem. Phys. 155 (1999) 223–247.
[30] J.X. Hu, Q. Xiao, A. Incecik, Passive locomotion and dynamic response of an asymmetric flapping foil, Presented at 21st International Offshore and Polar Engineering Conference, Maui, Hawaii, June 19–24, 2011.
[31] J.X. Hu, Q. Xiao, Passive locomotion for a self-propelled three-dimensional flapping wing, To be Presented at 22nd International Offshore and Polar Engineering Conference, Greece, June 19–22, 2012.
[32] G.J. Dong, X.Y. Lu, Numerical analysis on the propulsive performance and vortex shedding of fish-like travelling wavy plate, Internat. J. Numer. Methods Fluids 48 (2005) 1351–1373.